https://doi.org/10.5194/essd-2026-632
Preprint. Discussion started: 22 September 2026

Open Access Earth System Science Data Discussions

TEMPL: a Multi-Platform LiDAR Dataset of a Temperate Forest in the Eastern United States

Sangyoon Park [1], Zachary Nelson Horve[2], Cameron Patrick Wingren[2], Michael R Saunders[2], Chunxi Zhao[1], Sang-Yeop Shin[1], John Evan Flatt[2], Ayman Habib[1] and Songlin Fei[2]

[1]Lyles School of Civil and Construction Engineering, Purdue University, West Lafayette, IN 47907, United States
[2]Department of Forestry and Natural Resources, Purdue University, West Lafayette, IN 47907, United States

Correspondence to: Songlin Fei (sfei@purdue.edu)

Abstract. Laser scanning from multiple Light Detection and Ranging (LiDAR) platforms enables the acquisition of 3D point clouds from complementary sensing perspectives and at varying resolutions, supporting cross-platform forest measurement, point-cloud enhancement, tree species classification, and ecological analyses. However, publicly available multi-platform LiDAR datasets with corresponding individual-tree information remain scarce, particularly for temperate hardwood forests in the Central Hardwood Forest (CHF) region of the eastern United States. To address this gap, we collected data using an airborne LiDAR system (ALS), an uncrewed aerial vehicle LiDAR system (ULS), and two backpack LiDAR systems (BLS) in a temperate forest in the CHF of the eastern United States. The TEMPL dataset provides spatially well-aligned and georeferenced point clouds from multiple LiDAR platforms for nine continuous forest inventory (CFI) plots. A key feature of the dataset is the availability of corresponding individual-tree point clouds across multiple platforms, including 838 individual tree point clouds representing 231 trees from 16 tree species and a separate snag class. Associated tree attributes are also provided, including field-measured metrics and point-cloud-derived metrics estimated using quantitative structure models (QSMs). Together, these data provide a resource for cross-platform algorithm development and ecological analyses of tree structure within a forest region that is underrepresented in existing individual-tree LiDAR datasets. This paper describes the data acquisition, processing workflow, dataset contents, and potential applications. The entire dataset is available at https://doi.org/10.4231/5DGX-DP81.

1 Introduction

Light Detection and Ranging (LiDAR) remote sensing has greatly advanced our understanding of forest structure and composition worldwide in recent decades (Balestra et al., 2024; LaRue et al., 2023). LiDAR provides 3D representations of forest environments, enabling the derivation of detailed structural metrics such as diameter at breast height (DBH) (Hanafy et al., 2026), tree height (Laino et al., 2024), stem volume (Shao et al., 2026b), crown dimensions (Cheng et al., 2026), vertical foliage distribution (Yin et al., 2022), and above-ground biomass (AGB) (Thapa et al., 2025). Compared with traditional manual measurements, LiDAR offers equal or greater precision, substantially faster data acquisition, and greater spatial

https://doi.org/10.5194/essd-2026-632
Preprint. Discussion started: 22 September 2026

completeness across large geographic areas. As a result, LiDAR data have become a valuable resource for improving the accuracy, efficiency, and scalability of forest inventories.

In forestry applications, LiDAR systems are commonly classified according to sensing distance and platform type into airborne, near-proximal, and proximal categories. Airborne LiDAR systems (ALS) are typically mounted on crewed aircraft and acquire point clouds over large areas with relatively uniform coverage. This makes them well suited for landscape- and regional-scale mapping of canopy structure and terrain, although their point density is generally low, often below or around 100 points/m² depending on flight altitude. Near-proximal LiDAR systems are commonly deployed on uncrewed aerial vehicles and acquire data from positions close to and above the overstory canopy. Because they operate at lower flight altitudes than ALS, uncrewed aerial vehicle LiDAR systems (ULS) generally provide higher point densities and are particularly useful for stand-level surveys and canopy characterization. Proximal LiDAR systems acquire data from below the overstory canopy and include terrestrial LiDAR systems (TLS) and mobile LiDAR systems (MLS), such as backpack platforms. These systems generate dense under-canopy point clouds and capture detailed stem and lower-crown structure for tree-level measurement and monitoring. Figure 1 presents this conceptual grouping of forestry LiDAR mapping systems.

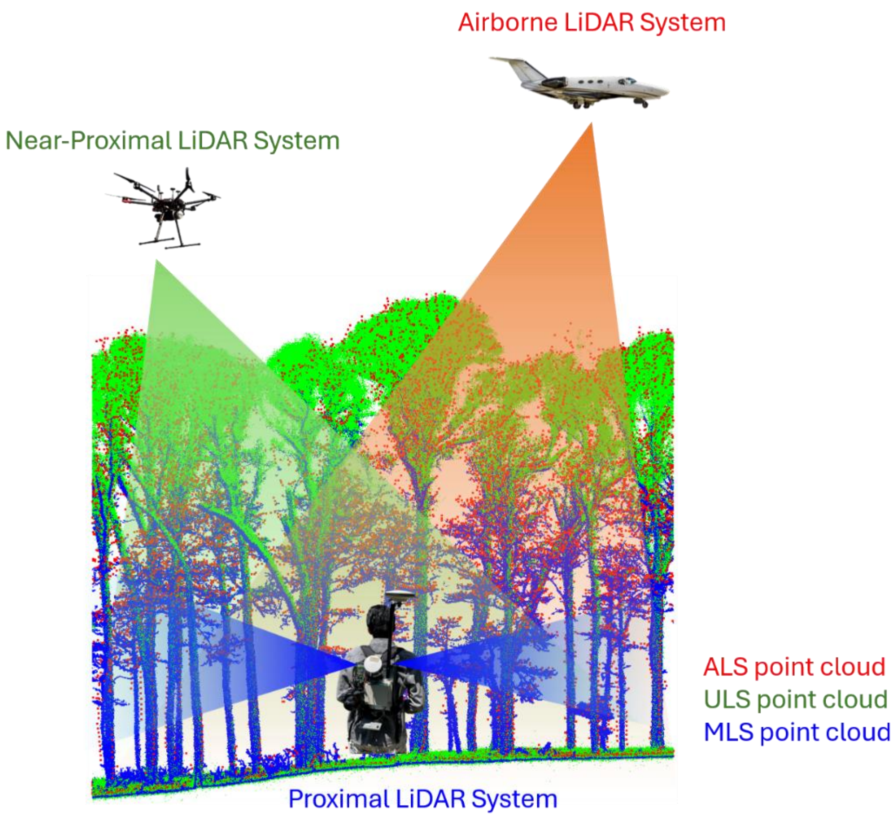

Figure 1: Schematic illustration of multi-platform LiDAR systems and representative point clouds acquired from airborne, near-proximal, and proximal perspectives in forest environments.

https://doi.org/10.5194/essd-2026-632
Preprint. Discussion started: 22 September 2026

Combining LiDAR data from complementary sensing perspectives can support the cross-platform transfer of structural information, including point-cloud super-resolution and completion (Shao et al., 2026a; Bornand et al., 2024), and provide benchmark data for learning-based tree species classification (Puliti et al., 2025). When linked to individual-tree field measurements and local stand context, such datasets can also support ecological analyses of tree architecture (Kröner et al., 2024) and broader forest inventory and carbon-monitoring applications (Romijn et al., 2015). They can further expand the geographic and taxonomic basis for comparing tree structural traits across forest regions (Jucker et al., 2025).

In recent years, notable progress has been made in LiDAR data acquisition using airborne (Gaydon and Roche, 2025), uncrewed aerial vehicle (Dubrovin et al., 2024), and backpack (Malladi et al., 2025) platforms. However, publicly available datasets acquired over the same forest area using multiple LiDAR platforms remain scarce. Existing examples have primarily focused on European and tropical forest sites (Weiser et al., 2022; Chavana-Bryant et al., 2026; Tebaldini et al., 2023), leaving temperate forests in eastern North America underrepresented. Weiser et al. provided georeferenced ALS, ULS, and TLS point clouds from 12 plots in two managed temperate mixed forests in southwestern Germany, characterized by central European tree species, multilayered stand structures, and dense forest cover (Weiser et al., 2022). Field measurements were available for six of the plots, and 77 trees had corresponding leaf-on ALS, ULS, and TLS point clouds together with field measurements. ForestScan (Chavana-Bryant et al., 2026) integrated ALS, ULS, TLS, and tree census data from tropical forests in French Guiana, Gabon, and Malaysian Borneo, including lowland terra firme rainforest, secondary and old-growth forests, and forests occurring on alluvial, sandstone, and kerangas soils. However, although the LiDAR and census data corresponded at the plot level, the study did not provide one-to-one links between field-measured trees and individual-tree point clouds across the LiDAR platforms. TomoSense (Tebaldini et al., 2023) provided ALS, ULS, backpack LiDAR system (BLS), TLS, and field inventory data from a heterogeneous temperate forest in the Eifel National Park, Germany, including beech- and oak-dominated deciduous stands, spruce stands, and forests spanning different topographic settings and age classes. However, individual-tree point clouds were provided only for the TLS data, and the study did not provide a quantitative assessment of cross-platform spatial alignment. In addition, the approximately two-year gap between the field inventory and LiDAR acquisitions may introduce temporal inconsistencies in tree-level comparisons. Thus, despite the growing availability of multi-platform forest LiDAR datasets, resources that combine spatially aligned point clouds for the same individual trees across multiple platforms with corresponding field measurements remain limited.

These existing datasets also leave an important geographic and structural gap in temperate hardwood forests of eastern North America. The Central Hardwood Forest (CHF) is one of the largest and most ecologically and economically important temperate forest regions in the eastern United States, supporting a substantial hardwood timber resource (~730.6 million m^3 of hardwood growing stock in Illinois, Indiana, and Missouri alone), forest-product industries contributing ~\$15.7 billion in GDP across these three states, and aboveground carbon stocks averaging ~40.9 Mg C ha^{-1} (Brandt et al., 2014; Oswalt et al., 2014; Jin et al., 2017). However, detailed individual-tree LiDAR datasets representing these forest structures remain limited compared with those available for European and tropical forests (Weiser et al., 2022; Yazdi et al., 2024; Griese et al., 2025; Puliti et al., 2025).

https://doi.org/10.5194/essd-2026-632
Preprint. Discussion started: 22 September 2026

In this paper, we present the TEMPL (Temperate Forest Multiplatform LiDAR) dataset, a multi-platform LiDAR dataset of a temperate forest in the CHF of the eastern United States that includes ALS, ULS, BLS, field inventory, and point-cloud-derived metric data. A defining feature of TEMPL is the provision of georeferenced and spatially aligned plot-level point clouds across ALS, ULS, and BLS, together with corresponding platform-specific individual-tree point clouds linked to a common field inventory comprising 231 trees. In addition, TEMPL is collocated with long-term continuous forest inventory (CFI) plots that have been repeatedly inventoried over three decades, and it includes all inventoried trees with DBH greater than 12.7 cm within the selected plots, an inventory protocol that is used nationwide for long-term forest monitoring. This complete inventory design places the detailed tree structure derived from LiDAR and the associated QSMs within a well-established forest inventory framework, providing information on neighboring trees and local stand context for each inventoried tree. The field measurements were also collected within approximately one year of the corresponding LiDAR acquisitions, thereby limiting temporal inconsistencies in tree-level comparisons. Together, these characteristics make TEMPL a resource for cross-platform forest measurement, algorithm development, and ecological analyses that link detailed tree architecture with field observations and local stand context. Specific research applications and the broader significance of the dataset are discussed in Section 5.

2 Study area and LiDAR systems

2.1 Test site

The TEMPL test site is located in an upland oak-hickory (*Quercus-Carya*) management compartment within the Martell Forest, West Lafayette, Indiana, United States. The area is characteristic of a mature, approximately 100-year-old CHF ecosystem, with dominant species including white, red, and black oak (*Q. alba, Q. rubra,* and *Q. velutina,* respectively); bitternut, pignut, and shagbark hickory (*C. cordiformis, C. glabra,* and *C. ovata,* respectively); tulip poplar (*Liriodendron tulipifera*); black walnut (*Juglans nigra*); and sugar maple (*Acer saccharum*), all of which are important timber species for the region. The forest contains a wide range of tree sizes, from young saplings to large, mature trees. Management of Martell Forest has been supported over the past several decades by an established forest inventory. Continuous forest inventory (CFI) plots, each covering 804.25 m^2 (0.08 ha) as a circular plot with a radius of 16 m, are distributed throughout the forest and have been remeasured regularly, generally on a 5- to 10-year cycle.

For TEMPL, nine CFI plots were selected. The plot center coordinates were updated by marking individual plot centers with targets and manually measuring them from UAV-derived aerial orthophotos acquired during the leaf-off season, which extends from November through April in this ecosystem (Carpenter et al., 2023). The spacing between CFI plots is approximately 80 m. A photograph of the study area is shown in Fig. 2.

https://doi.org/10.5194/essd-2026-632
Preprint. Discussion started: 22 September 2026

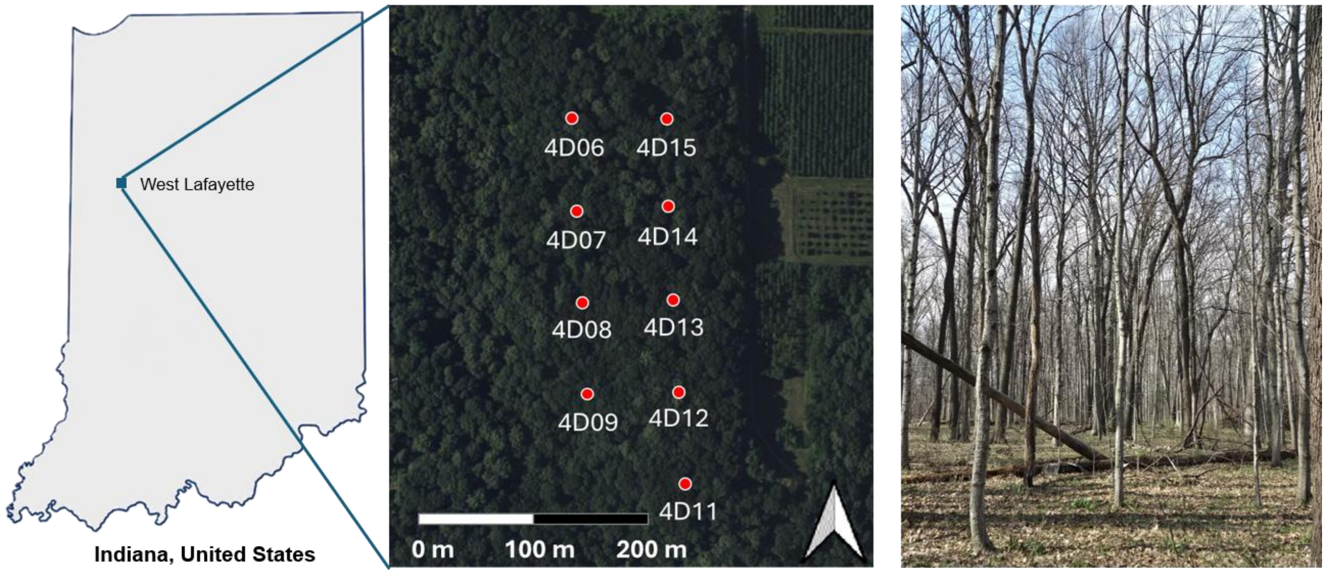

Figure 2: Locations of the forest plots in Martell Forest, West Lafayette, Indiana, United States, with a map and photograph of the study area.

2.2 LiDAR systems

This study used four datasets acquired from three types of LiDAR systems, including ALS from a crewed aircraft for airborne scanning, ULS for near-proximal scanning, and BLS for proximal scanning. The ALS and ULS data were collected using in-house developed systems at the Institute for Digital Forestry at Purdue University, while the BLS data were obtained using both an in-house developed system and a commercial system.

2.2.1 Airborne LiDAR system

An in-house developed ALS, the Purdue Airborne Mobile Mapping System (PAMMS), was used for airborne LiDAR data collection. As shown in Fig. 3a, the PAMMS consists of a RIEGL VUX-160 LiDAR unit and an Applanix POS AV 510 Global Navigation Satellite System/Inertial Navigation System (GNSS/INS) unit. The LiDAR data are directly georeferenced through the GNSS/INS unit, which records Inertial Measurement Unit (IMU) data at 200 Hz. After post-processing, the GNSS/INS unit provides trajectory accuracy of 2 cm horizontally and 5 cm vertically in position, 0.005° in roll/pitch angles, and 0.01° in heading under open-sky conditions. In this study, the ALS was calibrated using an automated universal multisensor advanced triangulation (AUMSAT) (Liu and Habib, 2026). Based on sensor specifications, the expected accuracy of the point cloud following calibration was estimated using a LiDAR Error Propagation Calculator (Habib et al., 2007). At a nominal flight altitude of 300 m above ground level, the expected point cloud accuracy is approximately 6 cm horizontal and 5 cm vertical at nadir, increasing to 9 cm horizontal and 7 cm vertical at the swath edges.

https://doi.org/10.5194/essd-2026-632
Preprint. Discussion started: 22 September 2026

2.2.2 UAV LiDAR system

An in-house developed ULS was used for near-proximal data collection. As shown in Fig. 3b, the ULS consists of an Ouster OS1-128 LiDAR unit and an Applanix APX15 v3 GNSS/INS unit mounted onboard a Freefly Systems Alta X. The LiDAR data are directly georeferenced through the GNSS/INS unit, which provides IMU measurements at 200 Hz. After post-processing, the GNSS/INS unit provides trajectory accuracy of 2–5 cm in position, 0.025° in roll/pitch angles, and 0.080° in heading under open-sky conditions. In this study, the ULS underwent a feature-based system calibration (Ravi et al., 2018). Using the same LiDAR error-propagation approach, the expected accuracy of the calibrated point cloud at a nominal flight altitude of 60 m was estimated to be 5–6 cm at nadir in both horizontal and vertical directions and 8–9 cm at the swath edges.

2.2.3 Backpack LiDAR system

Two BLS platforms were used for proximal data collection. The first BLS, BP-HDL32, is an in-house developed platform (Zhao et al., 2026). As shown in Fig. 3c, the BP-HDL32 system consists of a Velodyne HDL-32E LiDAR sensor and a NovAtel PwrPak7-E2 GNSS/INS unit. Direct georeferencing of the LiDAR is achieved through the GNSS/INS unit. The LiDAR sensor is mounted with its rotational axis inclined 40° from the vertical axis to improve the capture of upper-canopy structures relevant to forest inventory. The LiDAR sensor operates at 600 RPM, yielding a scan duration of 0.1 s per revolution. It has a maximum measurement range of 100 m and a range accuracy of approximately 2 cm.

The second BLS, Hovermap ST-X, is a commercial product developed by Emesent (Fig. 3d). The system uses a rotating LiDAR sensor with an angular field of view of 360° × 290°, enabling near-spherical coverage for simultaneous localization and mapping (SLAM). It has 32 LiDAR channels and a scanning rate of 640,000 points per second in single-return mode, with up to three returns available. Using its SLAM algorithm, the system provides a mapping accuracy of 1.5 cm under general conditions and a local accuracy standard deviation of 0.5 cm.

(a) (b)

https://doi.org/10.5194/essd-2026-632
Preprint. Discussion started: 22 September 2026

(c) (d)

Figure 3: LiDAR systems used in this study. (a) airborne LiDAR system, (b) UAV LiDAR system, and backpack LiDAR systems: (c) BP-HDL32 and (d) Hovermap ST-X.

3 Dataset

3.1 LiDAR data

To prepare the LiDAR data, point clouds from each system were reconstructed using different approaches tailored to the characteristics of each system. After reconstruction, the point clouds were clipped to a 25 m radius around the centers of the CFI plots to include a buffer beyond the nominal 16 m plot radius, as tree crowns can extend outside the plot boundary. All georeferenced point clouds are provided with horizontal coordinates in the NAD83(2011) / UTM zone 16N coordinate reference system (EPSG:6345), based on the GRS 1980 ellipsoid. Easting, northing, and ellipsoidal height values are expressed in meters.

3.1.1 ALS data

Since under-canopy features such as tree trunks are difficult to capture effectively during leaf-on conditions, ALS data were collected under leaf-off, snow-free conditions in March 2026 to ensure better visibility of these features. The dataset was acquired at a flight altitude of 300 m above ground level with a flight speed of 157.4 km/h. The flight mission consisted of four north-south flight lines, and the point clouds in neighboring flight lines had a 50% overlap. Figure 4a presents the ALS dataset, including a top view of the ALS trajectory obtained from GNSS/INS post-processing, the original point cloud, and the point cloud clipped around the CFI plots. Additional data details are summarized in Table 1.

3.1.2 ULS data

The ULS point cloud for this site was collected under leaf-off, snow-free conditions in February 2025 to effectively capture under-canopy features. To improve point cloud accuracy, only points within ±70° of nadir were reconstructed. The dataset was acquired at a flight altitude of 60 m above ground level and a flight speed of 10.8 km/h. The three flight missions consisted of

https://doi.org/10.5194/essd-2026-632
Preprint. Discussion started: 22 September 2026

a total of 24 east-west flight lines, with a lateral spacing of 20 m between adjacent lines. Figure 4b and Table 1 present the ULS dataset characteristics.

3.1.3 BLS data

BLS datasets were collected in January 2025 under leaf-off, snow-free conditions by walking through the study area to maximize tree coverage and improve the visibility of stem features. The BP-HDL32 and Hovermap ST-X systems were operated along trajectories that were designed to be as similar as possible; the two systems were carried sequentially along the same path during the same field session, with one operator following the other. For each system, four backpack missions were carried out along approximately orthogonal tracks across the test site.

Under-canopy forest environments present challenges for the BP-HDL32 system, including GNSS signal blockage and occlusions caused by dense canopy cover. These conditions reduce GNSS positioning accuracy and lead to trajectory drift. As a result, point cloud misalignments can occur, producing a ghosting effect in which the same tree appears duplicated because scans acquired at different times do not align spatially. To mitigate this issue, Integrated Scan Simultaneous Trajectory Enhancement and Mapping (IS^2-TEAM) (Zhao et al., 2026) was applied to individual scans to improve the trajectory and reconstruct a cleaner point cloud. This method achieved a mapping accuracy of 3 cm with a standard deviation of 1 cm. The trajectory enhancement was also applied to multiple adjacent missions collected in a large area, ensuring harmonized consolidation of cross-mission backpack LiDAR data to avoid misalignment in overlapping areas between adjacent missions, mainly due to mobile LiDAR trajectory drift. As a result, CFI plots located near different mission boundaries could be used while ensuring complete plot-level coverage by integrating adjacent missions. Figure 4c and Table 1 present the characteristics of the BLS (BP-HDL32) dataset.

Data captured by the Hovermap ST-X system were processed into point clouds using the SLAM workflow implemented in Emesent Aura software. The reconstructed point clouds were generated in a local coordinate system. Because the Aura-based processing workflow used in this study did not support harmonized multi-mission consolidation, full-mission registration alone could introduce residual misalignment in three plots (4D06, 4D08, and 4D13) located near overlapping areas between adjacent missions due to mobile LiDAR drift. Therefore, only the remaining six CFI plots fully covered by individual missions were used for the Hovermap ST-X dataset. To minimize the effect of mobile LiDAR drift, a plot-by-plot registration strategy was used to align the Hovermap ST-X point clouds to the corresponding georeferenced BP-HDL32 CFI plot point clouds. First, initial registration was performed for each mission by aligning the Hovermap ST-X mission point cloud to the corresponding BP-HDL32 mission point cloud using the iterative closest point (ICP) algorithm. For the six selected CFI plots, the Hovermap ST-X point clouds were then clipped using a 30 m radius from each plot center, including the nominal 25 m plot buffer plus an additional 5 m registration buffer. Each clipped plot-level point cloud was more precisely registered to the corresponding georeferenced BP-HDL32 CFI plot point cloud using ICP and finally clipped again to a 25 m radius, yielding the final six Hovermap ST-X CFI plot point clouds. Figure 4d and Table 1 present the characteristics of the BLS (Hovermap ST-X) dataset.

https://doi.org/10.5194/essd-2026-632
Preprint. Discussion started: 22 September 2026

Open Access Earth System Science Data Discussions

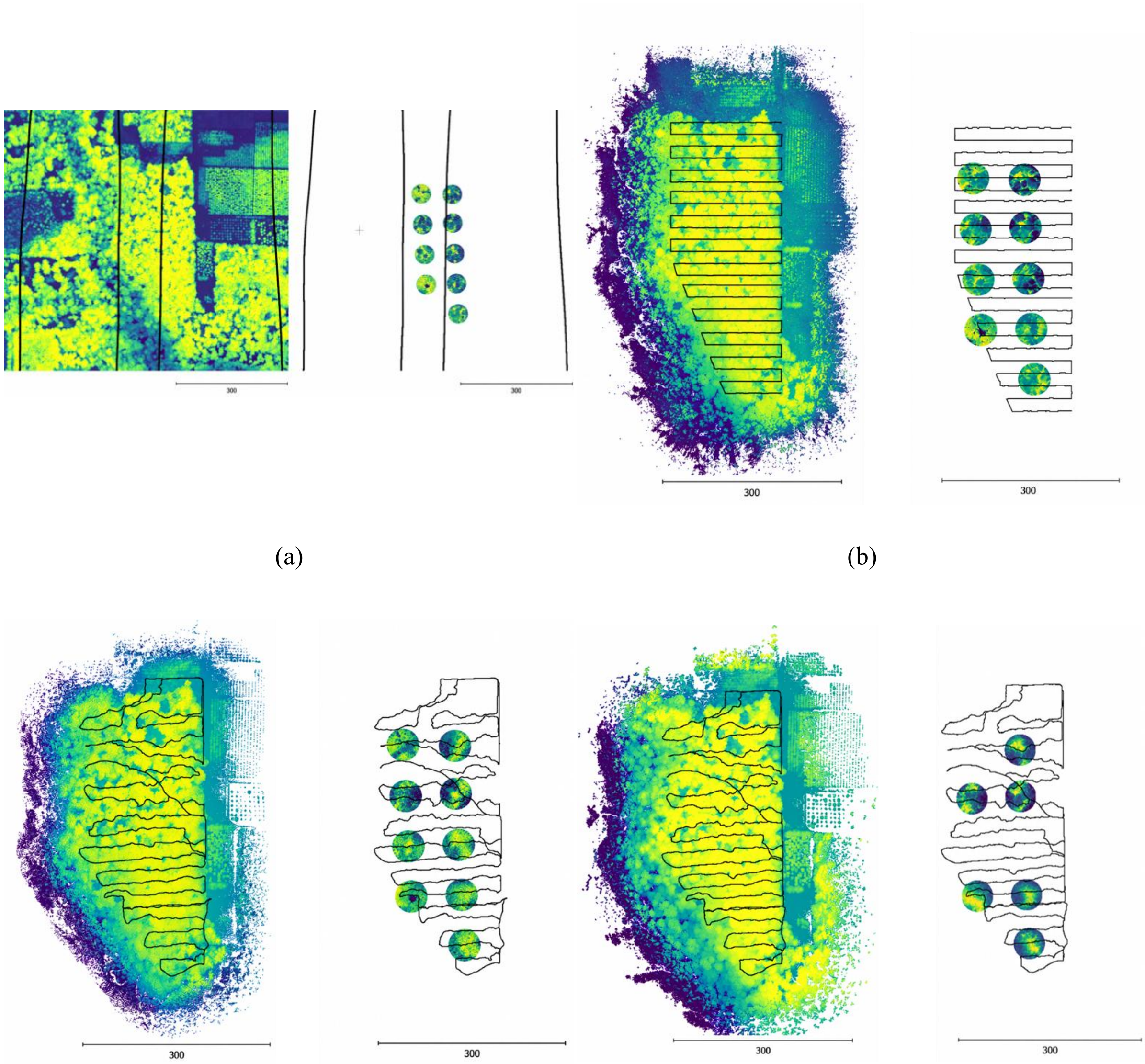

(a) (b) (c) (d)

Figure 4: Illustration of the LiDAR datasets. Each panel shows a top view of the trajectory of each LiDAR system (black line) overlaid on the collected point cloud (colored by height) and the point clouds clipped to a 25 m radius around the centers of the CFI plots (colored by height). Scale bars are in meters. (a) ALS dataset, (b) ULS dataset, BLS datasets: (c) BP-HDL32 and (d) Hovermap ST-X.

https://doi.org/10.5194/essd-2026-632
Preprint. Discussion started: 22 September 2026

Open Access Earth System Science Data Discussions

Table 1. Description of the LiDAR datasets

Dataset	ALS	ULS	BLS	
			BP-HDL32	Hovermap ST-X
Collection date	March 27, 2026	February 27, 2025	January 16, 2025	January 16, 2025
Number of CFI plots	9	9	9	6
Total CFI plot area including buffer	17,671.5 m^2	17,671.5 m^2	17,671.5 m^2	11,781 m^2
Total number of points	2,951,717	83,453,619	509,545,730	323,756,114
Average number of points per CFI plot	327,969	9,272,624	56,616,192	53,959,352
Average point density	167 points/m^2	4,722 points/m^2	28,834 points/m^2	27,481 points/m^2

3.2 Individual tree point clouds

Individual tree point clouds from all four LiDAR data sources, including ALS, ULS, and two BLS datasets, are provided for the 231 trees in TEMPL (Table 2). In total, 838 individual tree point clouds were extracted. Individual tree point clouds are provided as *.xyz ASCII text files and named according to their plot and tree IDs. Users can view the individually segmented trees for each LiDAR dataset (Fig. 5) or compare representative individual tree point clouds acquired from different platforms (Fig. 6).

Table 2. Number of individually segmented trees by CFI plot and LiDAR system

CFI plot	ALS*	ULS	BLS		Total
			BP-HDL32	Hovermap ST-X**	
4D06	24	24	24	N/A	72
4D07	28	28	28	28	112
4D08	31	31	31	N/A	93
4D09	23	23	23	23	92
4D11	39	40	40	40	159
4D12	26	27	27	27	107
4D13	29	29	29	N/A	87
4D14	15	15	15	15	60
4D15	14	14	14	14	56
Total	229	231	231	147	838

* Two trees were felled between the ULS/BLS and the ALS data acquisition dates.

** N/A indicates that no Hovermap ST-X point clouds are available for the corresponding plot.

https://doi.org/10.5194/essd-2026-632
Preprint. Discussion started: 22 September 2026

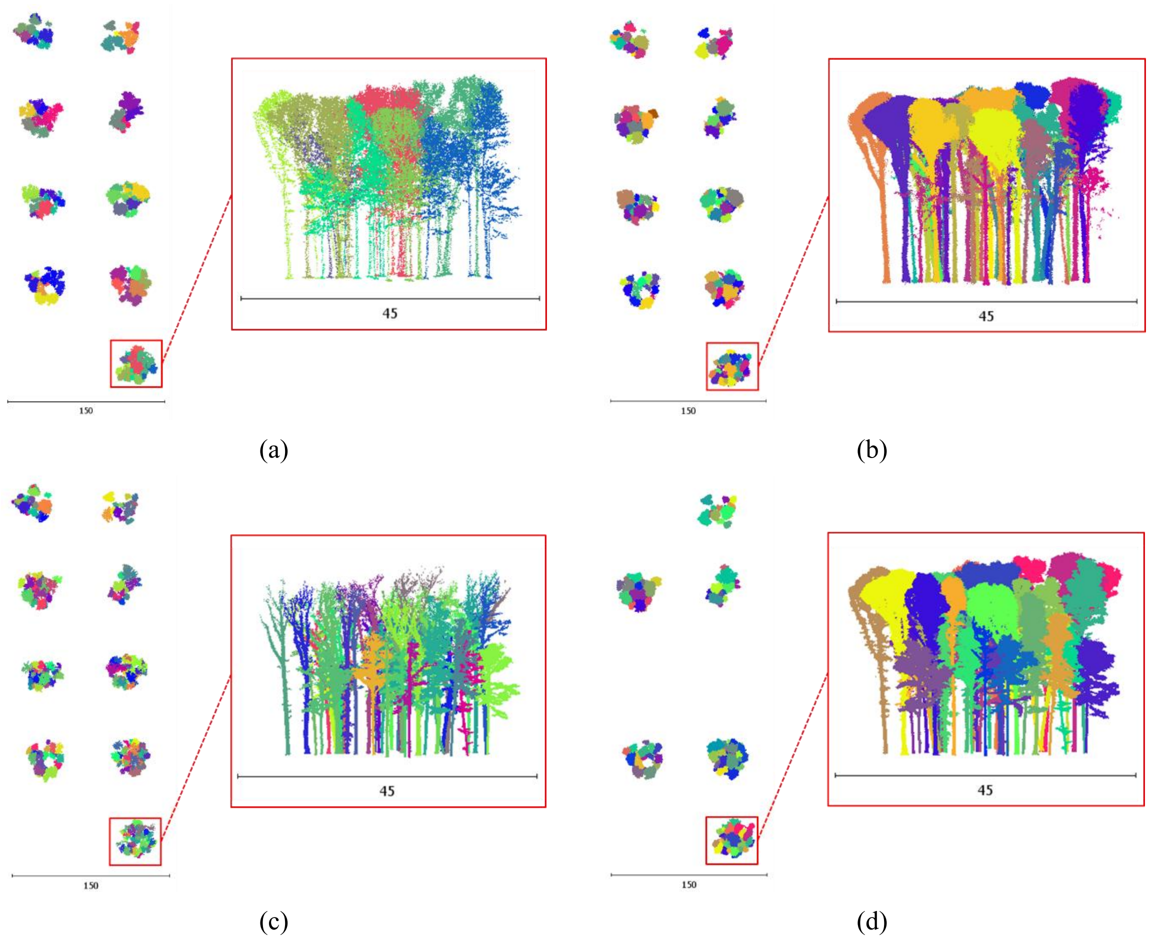

Figure 5: Illustration of the individual tree segmentation results. Each panel shows a top view of the tree point clouds (randomly colored by tree ID) in the CFI plots and a front view of the tree point clouds in a sample CFI plot. Scale bars are in meters. (a) ALS dataset, (b) ULS dataset, BLS datasets: (c) BP-HDL32 and (d) Hovermap ST-X.

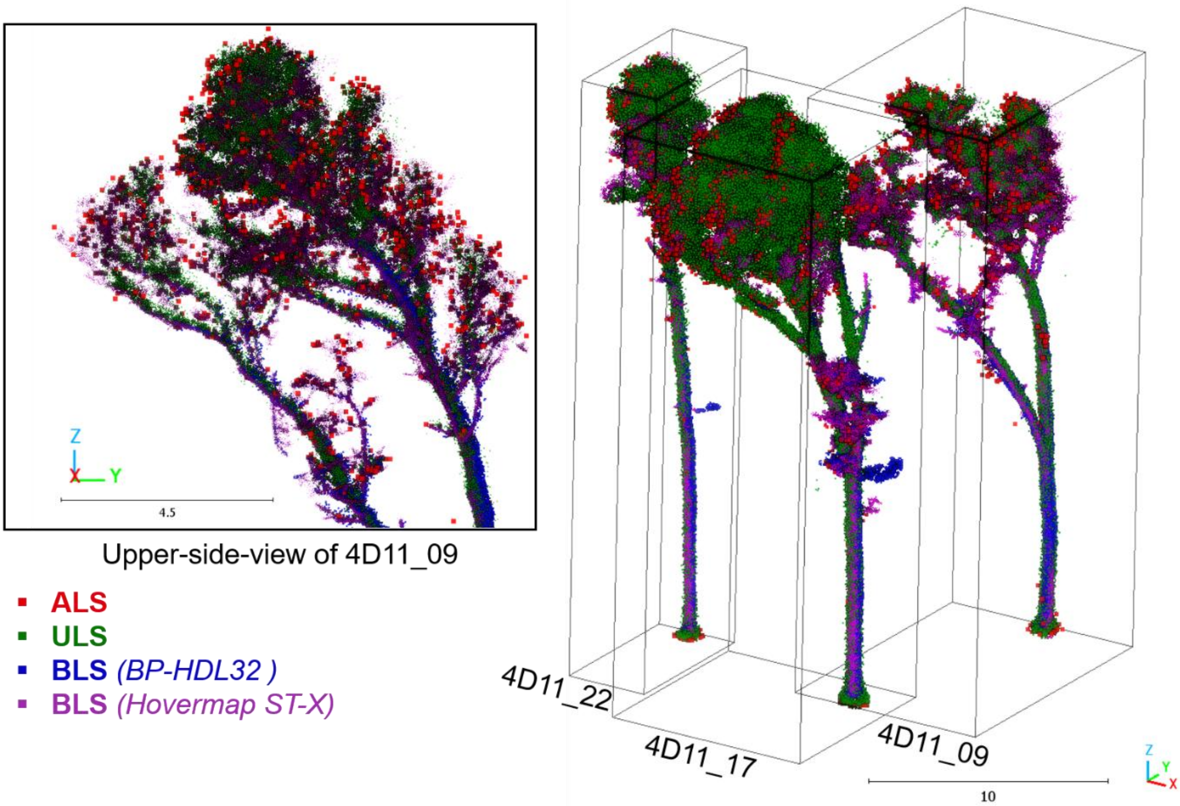

Figure 6: Example point clouds showing differences in point density and coverage across LiDAR platforms. Scale bars are in meters. Point clouds of three black oak trees in plot 4D11 are shown, and individual trees are labeled by their dataset tree IDs.

3.2.1 Tree segmentation from BLS (BP-HDL32 and Hovermap ST-X) point clouds

Individual tree segmentation for each plot was first performed automatically and subsequently improved through manual point-cloud editing. The automated segmentation followed a multi-stage geometric workflow (Hanafy et al., 2026). Ground points were first removed using a modified Cloth Simulation Filter (Liu and Habib, 2026). Intensity- and geometry-based filtering was then applied to extract woody components from the point cloud. DBSCAN clustering was used to detect individual tree trunks, and the detected trunks were used as seed regions for recovering the remaining tree points. Specifically, canopy points associated with each trunk were reassigned through a voxel-based KD-tree search, resulting in final individual tree segments. To further improve segmentation quality, the automatically generated tree segments were manually reviewed and refined using CloudCompare software.

3.2.2 Tree segmentation from ALS and ULS point clouds

Because the point clouds from all LiDAR systems were georeferenced and spatially aligned, the individual tree point clouds extracted from the BLS (BP-HDL32) data were used as reference tree segments to retrieve corresponding points from the ALS

https://doi.org/10.5194/essd-2026-632
Preprint. Discussion started: 22 September 2026

and ULS point clouds. A point-cloud-to-point-cloud matching approach was applied for this process. For each point in the ALS and ULS point clouds, the nearest point in the BLS-derived individual tree point clouds was first identified based on the 3D point-to-point distance. The horizontal distance between the query point and its nearest BLS tree point was then computed and used for tree-level assignment. This allowed points from the aerial platforms to be associated with the closest backpack-derived tree segment while accounting for vertical differences in canopy observation. The points assigned through this matching process formed the initial individual tree point clouds for the ALS and ULS datasets.

To account for differences in canopy visibility between ground-based and aerial LiDAR systems, a height-adaptive XY distance threshold was applied at the individual tree level. For each initial individual tree point cloud, the relative height of each point was normalized to a value between 0 and 1 based on the minimum and maximum elevations of the corresponding tree point cloud. Points with a relative height ratio below 0.7 were assigned to the lower tree portion, where BLS and ALS/ULS point clouds were expected to have stronger spatial correspondence. Points with a relative height ratio of 0.7 or higher were assigned to the upper-canopy portion, where ALS and ULS points could extend laterally beyond the BLS point clouds. XY distance thresholds of 0.2 m and 1.5 m were used for the lower and upper portions, respectively. Points satisfying the height-dependent XY distance threshold were assigned to the corresponding individual tree, whereas unmatched points were excluded from tree-level extraction. The extracted ALS and ULS tree point clouds were then visually inspected and manually refined using CloudCompare software.

3.3 Field measurements

Field measurements were conducted during the summer of 2025 across the nine CFI plots, representing a total area of 0.72 ha. DBH, tree location, and species were recorded for each inventoried tree. DBH was determined from the outside-bark circumference measured using a diameter tape at 1.37 m (4.5 ft) above ground. Tree locations were determined based on the measured distance and azimuth from the corresponding plot center. Snags were classified as a separate class. The species composition and stand structure of the nine CFI plots are summarized in Table 3. The plots included a total of 231 trees. Sugar maple was the most abundant species, whereas white oak and black oak accounted for the largest proportions of basal area because of their larger average DBH values. Field inventory records were linked to the corresponding individual tree point clouds using the common plot and tree IDs. Each tree point cloud was matched to the field inventory by comparing its location with the field-measured tree locations in CloudCompare. Tree metrics are provided as comma-separated values (CSV) files. Each file contains one row for each individual tree ID and one column for each tree metric.

https://doi.org/10.5194/essd-2026-632
Preprint. Discussion started: 22 September 2026

Open Access Earth System Science Data Discussions

Table 3. Species composition, average DBH, and basal area

Species	Common name	ID	Number of trees	Average DBH (cm)	Basal area (m² ha⁻¹)
Acer saccharum	Sugar Maple	SUM	78	21.41	4.49
Carya cordiformis	Bitternut Hickory	BIH	5	26.70	0.40
Carya glabra	Pignut Hickory	PIH	14	21.44	0.78
Carya ovata	Shagbark Hickory	SHH	3	24.30	0.20
Juglans nigra	Black Walnut	BLW	1	37.40	0.15
Liriodendron tulipifera	Tulip Poplar	YEP	13	58.85	5.23
Ostrya virginiana	Ironwood	IRO	1	15.90	0.03
Populus grandidentata	Bigtooth Aspen	BIA	3	49.33	0.84
Prunus serotina	Black Cherry	BLC	3	38.90	0.59
Quercus alba	White Oak	WHO	44	38.94	7.86
Quercus rubra	Northern Red Oak	REO	7	47.87	1.90
Quercus velutina	Black Oak	BLO	36	46.78	9.29
Sassafras albidum	Sassafras	SAS	4	20.58	0.19
Tilia americana	American Basswood	BAS	6	36.40	0.99
Ulmus americana	American Elm	AME	1	16.50	0.03
Ulmus rubra	Red Elm	REE	3	29.33	0.32
Snag		SNS	9	31.92	1.18
Total			231	33.27	34.52

3.4 Quantitative structure models

In addition to the field-measured tree metrics, point-cloud-derived metrics were estimated using quantitative structure models (QSMs). SmartQSM (Yang et al., 2026), a recent QSM approach that uses sparse-convolution-based point cloud contraction for individual tree reconstruction, was applied to each individually segmented tree point cloud from the BLS (BP-HDL32) data. Morphological and topological traits, including DBH, tree height, tree volume, stem length, and surface area, were derived from the reconstructed QSMs. QSM processing files, provided in MATLAB *.mat format, contain both the derived tree metrics and the reconstructed QSM-based tree models.

3.5 Data structure

The TEMPL dataset is organized by CFI plot, as illustrated in Fig. 7. Each top-level plot folder contains three primary data categories: field inventory, point clouds, and QSMs. The ‘Field_Inventory’ folder contains a CSV file named using the corresponding plot ID. The ‘Point_cloud’ folder is subdivided by LiDAR platform into ALS, ULS, and BLS. Each platform folder contains a plot-level point cloud in LAS format and an ‘Individual_Trees’ subfolder containing the corresponding individual-tree point clouds in XYZ format.

The BLS data are further separated by system. The ‘E2_HDL32’ folder is available for all nine plots, whereas the ‘Hovermap_STX’ folder is included only for the six plots acquired with that system. The QSM results are stored under ‘QSM/BLS/E2_HDL32/SmartQSM’ as MATLAB MAT files. Individual-tree point clouds and QSM files follow the naming

https://doi.org/10.5194/essd-2026-632
Preprint. Discussion started: 22 September 2026

convention ‘PlotID_TreeID’, such as 4D07_01.xyz and 4D07_01.mat. The same plot and tree identifiers are retained across the field inventory, platform-specific point clouds, and QSM results, allowing corresponding records to be linked directly.

```
PlotID
├── Field_Inventory
|   └── PlotID.csv
├── Point_cloud
|   ├── ALS
|   |   ├── PlotID.las
|   |   └── Individual_Trees
|   |       ├── PlotID_01.xyz
|   |       ├── PlotID_02.xyz
|   |       └── ...
|   ├── ULS
|   |   ├── PlotID.las
|   |   └── Individual_Trees
|   |       ├── PlotID_01.xyz
|   |       ├── PlotID_02.xyz
|   |       └── ...
|   └── BLS
|       ├── E2_HDL32
|       |   ├── PlotID.las
|       |   └── Individual_Trees
|       |       ├── PlotID_01.xyz
|       |       ├── PlotID_02.xyz
|       |       └── ...
|       └── Hovermap_STX
|           ├── PlotID.las
|           └── Individual_Trees
|               ├── PlotID_01.xyz
|               ├── PlotID_02.xyz
|               └── ...
└── QSM
    └── BLS
        └── E2_HDL32
            └── SmartQSM
                ├── PlotID_01.mat
                ├── PlotID_02.mat
                └── ...
```

Figure 7: Folder structure of the TEMPL dataset for a representative CFI plot. Each plot folder contains field inventory data, platform-specific plot-level and individual-tree point clouds, and QSM results.

4 Quality assessment

4.1 Cross-platform spatial alignment

Cross-platform spatial alignment was assessed at the individual-tree level using corresponding stem point clouds acquired by the different LiDAR platforms. For each BP-HDL32 individual tree point cloud, the stem segment between 1 and 2 m above ground was manually cropped. The corresponding stem points in the ALS, ULS, and Hovermap ST-X BLS individual tree point clouds were then manually extracted using the same absolute elevation range. For each tree, the 3D point-to-point distance from each ALS, ULS, and Hovermap ST-X BLS stem point to its nearest point in the corresponding BP-HDL32 BLS stem point cloud was calculated and used to assess cross-platform spatial alignment. The mean and RMSE of these distances were first calculated for each tree. The mean and standard deviation (SD) of the tree-level mean distances and RMSE values, together with the median of the tree-level mean distances, were then summarized for each platform comparison in Table 4.

The Hovermap ST-X and BP-HDL32 datasets showed the smallest 3D point-to-point differences, with a mean tree-level distance of 1.52 ± 0.57 cm, a median tree-level mean distance of 1.40 cm, and a mean tree-level RMSE of 1.87 ± 0.69 cm. The corresponding mean tree-level distances were 3.66 ± 1.10 cm for ALS and 3.75 ± 0.62 cm for ULS, while the median tree-

https://doi.org/10.5194/essd-2026-632
Preprint. Discussion started: 22 September 2026

level mean distances were 3.57 and 3.73 cm, respectively. The mean tree-level RMSE values were 4.40 ± 1.16 cm for ALS and 4.60 ± 0.62 cm for ULS. These results indicate greater cross-platform spatial agreement between the two BLS datasets, whereas the ALS and ULS datasets showed comparable agreement with the BP-HDL32 reference point clouds. The measured differences may also reflect variations in point density, occlusion, and acquisition timing among the platforms.

Table 4. Summary of 3D point-to-point distances between platform-specific stem point clouds and the BP-HDL32 BLS reference point clouds.

Comparison	Tree-level mean distance, mean ± SD (cm)	Tree-level mean distance, median (cm)	Tree-level RMSE, mean ± SD (cm)
ALS to BP-HDL32 BLS	3.66 ± 1.10	3.57	4.40 ± 1.16
ULS to BP-HDL32 BLS	3.75 ± 0.62	3.73	4.60 ± 0.62
Hovermap ST-X BLS to BP-HDL32 BLS	1.52 ± 0.57	1.40	1.87 ± 0.69

4.2 Point-cloud-derived estimates and field measurements

To assess the agreement between point-cloud-derived estimates and field measurements, QSM-derived DBH values obtained from the BP-HDL32 BLS data were compared with the corresponding field-measured DBH values for 231 trees. The RMSE, coefficient of determination (R^2), and bias were used as evaluation metrics. Bias was calculated as the QSM-derived DBH minus the field-measured DBH. Reduced major axis (RMA) regression was used because both the field measurements and QSM-derived estimates may contain measurement uncertainty, unlike ordinary least-squares regression, which assumes that the independent variable is measured without error.

As shown in Fig. 8a, the QSM-derived and field-measured DBH values exhibited a strong linear relationship, with an R^2 of 0.97. The RMSE was 2.79 cm, indicating that the overall differences between the two sets of measurements were relatively small. The bias was −0.53 cm, indicating a slight overall underestimation of DBH by the QSM-derived values. This negative bias may partly reflect differences in how DBH was measured and derived. Field-measured DBH was determined from the outside-bark circumference using a diameter tape, whereas QSM-derived DBH was calculated from the reconstructed trunk geometry informed by stem-surface points representing both recessed and protruding portions of the bark.

To further evaluate the estimates at practically relevant error thresholds, an individual-tree error-tolerance curve was generated using the absolute DBH error for each tree. As shown in Fig. 8b, 67.1% of the QSM-derived estimates were within 1 inch (2.54 cm) of the corresponding field measurements, while 92.6% were within 2 inches (5.08 cm). Thus, more than two-thirds of the estimates differed from the field measurements by less than 1 inch, and more than 90% differed by less than 2 inches. These results demonstrate that the BP-HDL32 individual tree point clouds and their associated QSM products provide DBH estimates that are generally consistent with the field inventory measurements.

https://doi.org/10.5194/essd-2026-632
Preprint. Discussion started: 22 September 2026

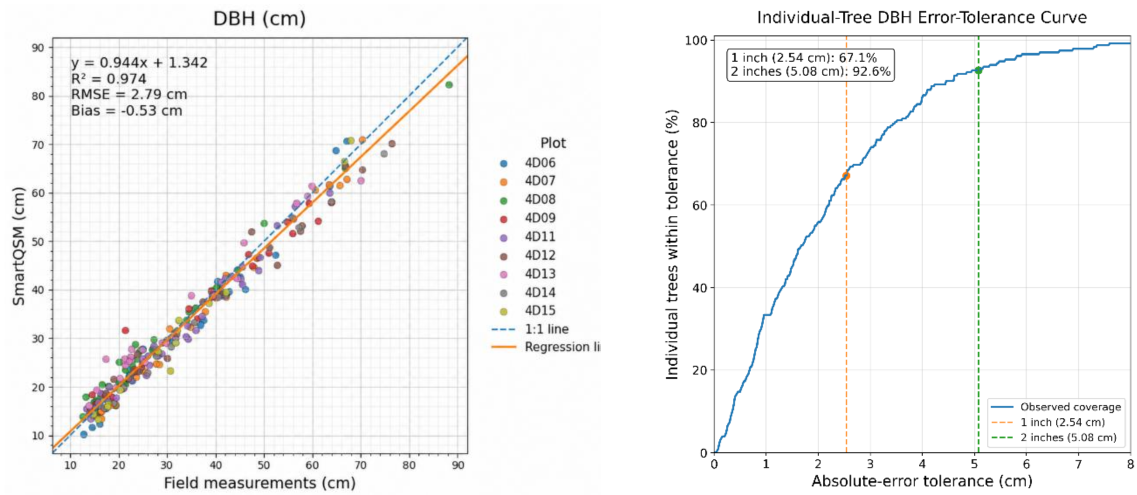

(a) (b)

Figure 8: Comparison of point-cloud-derived DBH from the BLS (BP-HDL32) data and field-measured DBH values: (a) scatter plot with the 1:1 reference and fitted RMA regression lines; and (b) individual-tree DBH error-tolerance curve showing the proportion of estimates within predefined absolute-error tolerances.

5 Potential applications and broader significance

5.1 Cross-platform enhancement and scaling of forest LiDAR data

For remote sensing scientists, TEMPL provides a useful resource for developing and evaluating methods that transfer information across LiDAR platforms and spatial resolutions. Because the same individual trees are represented by spatially aligned point clouds from multiple platforms, dense BLS point clouds can provide detailed structural information for developing and testing super-resolution approaches that enhance lower-density LiDAR point clouds (e.g., ALS and ULS) by increasing point density and recovering finer structural details. The paired individual-tree point clouds can also support the development and evaluation of tree point-cloud completion methods. Airborne LiDAR point clouds often provide incomplete representations of individual trees because of occlusion, uneven point density, and limited sampling of stems and branches, and several studies have explored methods for reconstructing missing tree structures from incomplete point clouds (Bornand et al., 2024; Luo et al., 2026). In TEMPL, the spatially aligned and generally more detailed BLS point clouds can provide reference representations for evaluating how effectively such methods recover missing geometric information from ALS or ULS point clouds. Improvements in super-resolution and point-cloud completion could support the retrieval of stem positions and tree biometric attributes such as DBH and stem volume from lower-density ALS or ULS point clouds over broader spatial extents (Shao et al., 2026a). Because forest inventories are often constrained by the cost and spatial coverage of high-resolution measurements, improved information retrieval from ALS and ULS point clouds could contribute to regional- and national-scale biomass assessment and forest carbon monitoring (Romijn et al., 2015). The corresponding point clouds across platforms also provide a basis for developing and evaluating scaling relationships between detailed tree-level information derived from

https://doi.org/10.5194/essd-2026-632
Preprint. Discussion started: 22 September 2026

proximal LiDAR and structural information obtainable from airborne platforms. Such relationships could help determine which fine-scale tree attributes can be reliably transferred across sensing platforms and resolutions.

5.2 Species classification

LiDAR-based tree species classification is an important research priority, but learning-based approaches remain constrained by the limited availability of labeled training data. The multi-platform nature of TEMPL provides a useful resource for developing and evaluating such methods. Many existing benchmark datasets provide data from a single platform (Seidel et al., 2021), while multi-platform datasets do not necessarily provide point clouds of the same individual trees across platforms, limiting direct evaluation of algorithm performance under different sensing conditions (Puliti et al., 2025). In addition, forests of the eastern United States are poorly represented in existing benchmark datasets (Weiser et al., 2022; Puliti et al., 2025). TEMPL therefore provides an opportunity to test the transferability and generalizability of classification approaches to species and structural forms that are underrepresented in current benchmark and training datasets.

5.3 Ecological applications

Beyond these algorithmic applications, TEMPL provides opportunities to investigate relationships between individual-tree structure and ecological attributes. The combination of detailed three-dimensional tree structure, species information, tree size, and plot-level inventory data allows tree architecture to be examined in relation to local stand context and neighboring trees. Recent studies have linked tree structural traits to radial growth in several European tree species, providing new insights into relationships among tree architecture, competition, and productivity (Kröner et al., 2024; Ahmed et al., 2025). Because the TEMPL plots are part of a long-term continuous forest inventory network, linking TEMPL with historical or future inventory records could provide opportunities to test whether relationships between tree architecture and growth identified primarily in European forests also apply to temperate hardwood forests of eastern North America. Planned future field measurements and LiDAR acquisitions will further support analyses of changes in tree structure, growth, mortality, and stand dynamics over time.

5.4 Broader scientific significance

Finally, TEMPL contributes to the growing availability of high-resolution individual-tree LiDAR data for studying tree architectural traits. LiDAR-derived structural traits are increasingly being used to investigate broader relationships among tree form, species strategies, and ecosystem functioning (Verbeeck et al., 2019; Laurans et al., 2024; Jucker et al., 2025). Publicly available datasets with species labels and quantitative structure models remain strongly concentrated in Europe (Yazdi et al., 2024; Griese et al., 2025). By adding point clouds from the CHF region of the eastern United States, TEMPL expands the geographic and taxonomic coverage available for cross-region comparisons and broader syntheses of tree architectural traits and their ecological relationships.

https://doi.org/10.5194/essd-2026-632
Preprint. Discussion started: 22 September 2026

Open Access Earth System Science Data Discussions

6 Conclusion

The TEMPL dataset provides spatially well-aligned and georeferenced multi-resolution point clouds acquired from airborne, UAV, and backpack LiDAR systems in a temperate forest in eastern North America. The combination of CFI plot point clouds, segmented individual tree point clouds, field inventory measurements, and point-cloud-derived tree attributes supports research on tree detection, segmentation, species classification, biometric estimation, point-cloud super-resolution and completion, and cross-platform scaling across multiple sensing perspectives and spatial resolutions. Because the CFI plots at Martell Forest are remeasured regularly, generally on a 5- to 10-year cycle, future updates to TEMPL will incorporate repeated field measurements and LiDAR acquisitions. These additions will support analyses of changes in forest structure over time and comparisons of multi-platform LiDAR point clouds across acquisition dates. The dataset will also be expanded to include additional CFI plots, individual tree point clouds, and point-cloud-derived attributes, further increasing its value for forestry and remote sensing research.

Data availability

The entire dataset is freely available through the Data-to-Science (D2S) platform (Jung et al., 2026) and can be accessed at https://doi.org/10.4231/5DGX-DP81 (Park et al., 2026).

Author contributions

Conceptualization: S.P. and S.F.; Data curation: S.P. and Z.N.H.; Formal analysis: S.P. and Z.N.H.; Funding acquisition: A.H. and S.F.; Investigation: S.P., Z.N.H., C.P.W., M.R.S., C.Z., S.-Y.S., and J.E.F.; Methodology: S.P., A.H., and S.F.; Project administration: A.H. and S.F.; Resources: A.H. and S.F.; Software: S.P., C.Z., and S.-Y.S.; Supervision: A.H. and S.F.; Validation: S.P. and Z.N.H.; Visualization: S.P.; Writing (original draft preparation): S.P.; Writing (review and editing): All authors.

Competing interests

The contact author has declared that none of the authors has any competing interests.

Disclaimer

Copernicus Publications remains neutral with regard to jurisdictional claims made in the text, published maps, institutional affiliations.

https://doi.org/10.5194/essd-2026-632
Preprint. Discussion started: 22 September 2026

Financial support

This work is partially supported by the U.S. Department of Agriculture's National Institute of Food and Agriculture (project award nos. 2023-68012-38992 and 2024-67021-42879). Any opinions, findings, conclusions, or recommendations expressed in this publication are those of the author(s) and should not be construed to represent any official USDA or U.S. Government determination or policy.

Review statement

The review statement will be added by Copernicus Publications listing the handling editor as well as all contributing referees according to their status anonymous or identified.

References

Emesent Aura: https://www.emesent.com/emesent-product/emesent-aura/, last access: June 30, 2026.

CloudCompare: https://www.cloudcompare.org/, last access: June 30, 2026.

Ahmed, S., Hilmers, T., Uhl, E., Tupinambá-Simões, F., Bravo, F., del Río, M., and Pretzsch, H.: Crown structure indicates tree secondary growth, competition legacy, and growth potential of dominant species in Europe, Ecological Indicators, 170, 113074, https://doi.org/10.1016/j.ecolind.2025.113074, 2025.

Balestra, M., Marselis, S., Sankey, T. T., Cabo, C., Liang, X., Mokroš, M., Peng, X., Singh, A., Stereńczak, K., Vega, C., Vincent, G., and Hollaus, M.: LiDAR Data Fusion to Improve Forest Attribute Estimates: A Review, Curr. For. Rep., 10, 281-297, https://doi.org/10.1007/s40725-024-00223-7, 2024.

Bornand, A., Abegg, M., Morsdorf, F., and Rehush, N.: Completing 3D point clouds of individual trees using deep learning, Methods in Ecology and Evolution, 15, 2010-2023, https://doi.org/10.1111/2041-210X.14412, 2024.

Brandt, L., He, H., Iverson, L., Thompson, F. R., Butler, P., Handler, S., Janowiak, M., Shannon, P. D., Swanston, C., Albrecht, M., Blume-Weaver, R., Deizman, P., DePuy, J., Dijak, W. D., Dinkel, G., Fei, S., Jones-Farrand, D. T., Leahy, M., Matthews, S., Nelson, P., Oberle, B., Perez, J., Peters, M., Prasad, A., Schneiderman, J. E., Shuey, J., Smith, A. B., Studyvin, C., Tirpak, J. M., Walk, J. W., Wang, W. J., Watts, L., Weigel, D., and Westin, S.: Central Hardwoods ecosystem vulnerability assessment and synthesis: a report from the Central Hardwoods Climate Change Response Framework project, U.S. Department of Agriculture, Forest Service, Northern Research Station, 10.2737/nrs-gtr-124, 2014.

Carpenter, J., Rentauskas, D., Makkar, N., Jung, J., and Fei, S.: Improving Deciduous Forest Inventory Plot Center Measurement Using Unoccupied Aerial Systems Imagery, J. For., 121, 262-271, https://doi.org/10.1093/jofore/fvad008, 2023.

Chavana-Bryant, C., Wilkes, P., Yang, W., Burt, A., Vines, P., Bennett, A. C., Pickavance, G. C., Cooper, D. L. M., Lewis, S. L., Phillips, O. L., Brede, B., Lau, A., Herold, M., McNicol, I. M., Mitchard, E. T. A., Coomes, D. A., Jackson, T. D., Makaga, L., Milamizokou Napo, H. O., Ngomanda, A., Ntie, S., Medjibe, V., Dimbonda, P., Soenens, L., Daelemans, V., Proux, L.,

https://doi.org/10.5194/essd-2026-632
Preprint. Discussion started: 22 September 2026

Open Access Earth System Science Data Discussions

Nilus, R., Labrière, N., Jeffery, K., Burslem, D. F. R. P., Clewley, D., Moffat, D., Qie, L., Bartholomeus, H., Vincent, G., Barbier, N., Derroire, G., Abernethy, K., Scipal, K., and Disney, M.: ForestScan: a unique multiscale dataset of tropical forest structure across 3 continents including terrestrial, UAV and airborne LiDAR and in-situ forest census data, Earth Syst. Sci. Data, 18, 1243-1274, https://doi.org/10.5194/essd-18-1243-2026, 2026.

Cheng, S., Hao, Y., Liu, J., Liu, X., Dong, L., Zhao, Y., and Li, F.: Beyond crown volume: UAV-LiDAR-derived foliated crown volume (FCV) enhances coniferous tree attribute estimation, Comput. Electron. Agric., 245, 111555, https://doi.org/10.1016/j.compag.2026.111555, 2026.

Dubrovin, I., Fortin, C., and Kedrov, A.: An open dataset for individual tree detection in UAV LiDAR point clouds and RGB orthophotos in dense mixed forests, Sci. Rep., 14, 21938, https://doi.org/10.1038/s41598-024-72669-5, 2024.

Gaydon, C. and Roche, F.: PureForest: A Large-Scale Aerial Lidar and Aerial Imagery Dataset for Tree Species Classification in Monospecific Forests, 2025 IEEE/CVF Winter Conference on Applications of Computer Vision (WACV), 26 Feb.-6 March, 5895-5904, https://doi.org/10.1109/WACV61041.2025.00575, 2025.

Griese, N., Ritzert, M., and Nölke, N.: A large dataset of labelled single tree point clouds, QSMs and tree graphs, Scientific Data, 12, 1953, https://doi.org/10.1038/s41597-025-06421-7, 2025.

Habib, A. F., Bang, K. I., Shin, S.-W., and Mitishita, E.: LiDAR system self-calibration using planar patches from photogrammetric data, The Fifth International Symposium on Mobile Mapping Technology (MMT'07), 2007.

Hanafy, H., Park, S., Fei, S., and Habib, A.: A Unified Framework for Individual Tree Segmentation and Forest Biometrics Derivation from LiDAR Point Clouds Captured by Different Platforms in Diverse Forest Environments, Remote Sens., 18, 3059, https://doi.org/10.3390/rs18173059, 2026.

Jin, W., He, H. S., Thompson, F. R., Wang, W. J., Fraser, J. S., Shifley, S. R., Hanberry, B. B., and Dijak, W. D.: Future forest aboveground carbon dynamics in the central United States: the importance of forest demographic processes, Sci. Rep., 7, 41821, https://doi.org/10.1038/srep41821, 2017.

Jucker, T., Fischer, F. J., Chave, J., Coomes, D. A., Caspersen, J., Ali, A., Loubota Panzou, G. J., Feldpausch, T. R., Falster, D., Usoltsev, V. A., Jackson, T. D., Adu-Bredu, S., Alves, L. F., Aminpour, M., Angoboy Ilondea, B., Anten, N. P. R., Antin, C., Askari, Y., Ayyappan, N., Banin, L. F., Barbier, N., Battles, J. J., Beeckman, H., Bocko, Y. E., Bond-Lamberty, B., Bongers, F., Bowers, S., van Breugel, M., Chantrain, A., Chaudhary, R., Dai, J., Dalponte, M., Dimobe, K., Domec, J.-C., Doucet, J.-L., Dupuy Rada, J. M., Duursma, R. A., Enríquez, M., van Ewijk, K. Y., Farfán-Rios, W., Fayolle, A., Ferretti, M., Forni, E., Forrester, D. I., Gilani, H., Godlee, J. L., Haeni, M., Hall, J. S., He, J.-K., Hemp, A., Hernández-Stefanoni, J. L., Higgins, S. I., Holdaway, R. J., Hussain, K., Hutley, L. B., Ichie, T., Iida, Y., Jiang, H.-S., Joshi, P. R., Kaboli, H., Kazempour Larsary, M., Kenzo, T., Kloeppel, B. D., Kohyama, T. S., Kunwar, S., Kuyah, S., Kvasnica, J., Lin, S., Lines, E. R., Liu, H., Lorimer, C., Loumeto, J.-J., Malhi, Y., Marshall, P. L., Mattsson, E., Matula, R., Meave, J. A., Mensah, S., Mi, X., Momo, S. T., Moncrieff, G. R., Mora, F., Muñoz, R., Nissanka, S. P., Nur Hajar, Z. S., O'Hara, K. L., Pearce, S., Pelissier, R., Peri, P. L., Ploton, P., Poorter, L., Pour, M. J., Pourbabaei, H., Ribeiro, S. C., Ryan, C., Sanaei, A., Sanger, J., Schlund, M., Sellan, G., Shenkin, A., Sonké, B., Sterck, F. J., Svátek, M., Takagi, K., Trugman, A. T., Vadeboncoeur, M. A., Valipour, A., Vanderwel,

M. C., Vovides, A. G., Waldner, P., Wang, W., Wang, L.-Q., Wirth, C., Woods, M., Xiang, W., de Aquino Ximenes, F., Xu, Y., Yamada, T., Zavala, M. A., and Zimmermann, N. E.: The global spectrum of tree crown architecture, Nature Communications, 16, 4876, https://doi.org/10.1038/s41467-025-60262-x, 2025.

Jung, M., Hancock, B. G., Qian, Z. C., Zhuo, N., Gong, Z., Doucette, J. S., and Jung, J.: Data-to-Science (D2S): An open-source ecosystem for collaborative geospatial data science research, J. Open Source Softw., 11, 9497, https://doi.org/10.21105/joss.09497, 2026.

Kröner, K., Larysch, E., Schindler, Z., Obladen, N., Frey, J., Stangler, D. F., and Seifert, T.: Influence of crown morphology and branch architecture on tree radial growth of drought-affected Fagus sylvatica L, Forest Ecosystems, 11, 100237, https://doi.org/10.1016/j.fecs.2024.100237, 2024.

Laino, D., Cabo, C., Prendes, C., Janvier, R., Ordonez, C., Nikonovas, T., Doerr, S., and Santin, C.: 3DFin: a software for automated 3D forest inventories from terrestrial point clouds, Forestry, 97, 479-496, https://doi.org/10.1093/forestry/cpae020, 2024.

LaRue, E. A., Fahey, R. T., Alveshere, B. C., Atkins, J. W., Bhatt, P., Buma, B., Chen, A., Cousins, S., Elliott, J. M., Elmore, A. J., Hakkenberg, C. R., Hardiman, B. S., Johnson, J. S., Kashian, D. M., Koirala, A., Papeş, M., St Hilaire, J. B., Surasinghe, T. D., Zambrano, J., Zhai, L., and Fei, S.: A theoretical framework for the ecological role of three-dimensional structural diversity, Front. Ecol. Environ., 21, 4-13, https://doi.org/10.1002/fee.2587, 2023.

Laurans, M., Munoz, F., Charles-Dominique, T., Heuret, P., Fortunel, C., Isnard, S., Sabatier, S.-A., Caraglio, Y., and Violle, C.: Why incorporate plant architecture into trait-based ecology?, Trends in Ecology & Evolution, 39, 524-536, https://doi.org/10.1016/j.tree.2023.11.011, 2024.

Liu, J. and Habib, A.: Automated Enhancement of Multimodal Geospatial Data Alignment Through System Calibration and Trajectory Refinement, IEEE J. Sel. Top. Appl. Earth Obs. Remote Sens., 19, 2233-2253, https://doi.org/10.1109/JSTARS.2025.3643441, 2026.

Luo, B., Yang, J., Shi, S., Gan, R., Wu, Z., Wang, S., Wang, A., Du, L., and Gong, W.: InceptionFormer: A deep learning framework for UAV LiDAR point cloud completion to improve tree parameters estimation in dense forests, Remote Sens. Environ., 338, 115348, https://doi.org/10.1016/j.rse.2026.115348, 2026.

Malladi, M. V. R., Chebrolu, N., Scacchetti, I., Lobefaro, L., Guadagnino, T., Casseau, B., Oh, H., Freißmuth, L., Karppinen, M., Schweier, J., Leutenegger, S., Behley, J., Stachniss, C., and Fallon, M.: Digiforests: a Longitudinal Lidar Dataset for Forestry Robotics, 2025 IEEE International Conference on Robotics and Automation (ICRA), 19-23 May, 1459-1466, https://doi.org/10.1109/ICRA55743.2025.11128697, 2025.

Oswalt, S. N., Smith, W. B., Miles, P. D., and Pugh, S. A.: Forest Resources of the United States, 2012: a technical document supporting the Forest Service 2010 update of the RPA Assessment, U.S. Department of Agriculture, Forest Service, 10.2737/wo-gtr-91, 2014.

https://doi.org/10.5194/essd-2026-632
Preprint. Discussion started: 22 September 2026

Park, S., Horve, Z. N., Wingren, C. P., Saunders, M. R., Zhao, C., Shin, S.-Y., Flatt, J. E., Habib, A., and Fei, S.: TEMPL: Temperate Forest Multiplatform LiDAR, Purdue University Research Repository [data set], https://doi.org/10.4231/5DGX-DP81, 2026.

Puliti, S., Lines, E. R., Müllerová, J., Frey, J., Schindler, Z., Straker, A., Allen, M. J., Winiwarter, L., Rehush, N., Hristova, H., Murray, B., Calders, K., Coops, N., Höfle, B., Irwin, L., Junttila, S., Krůček, M., Krok, G., Král, K., Levick, S. R., Luck, L., Missarov, A., Mokroš, M., Owen, H. J. F., Stereńczak, K., Pitkänen, T. P., Puletti, N., Saarinen, N., Hopkinson, C., Terryn, L., Torresan, C., Tomelleri, E., Weiser, H., and Astrup, R.: Benchmarking tree species classification from proximally sensed laser scanning data: Introducing the FOR-species20K dataset, Methods in Ecology and Evolution, 16, 801-818, https://doi.org/10.1111/2041-210X.14503, 2025.

Ravi, R., Lin, Y. J., Elbahnasawy, M., Shamseldin, T., and Habib, A.: Simultaneous System Calibration of a Multi-LiDAR Multicamera Mobile Mapping Platform, IEEE J. Sel. Top. Appl. Earth Obs. Remote Sens., 11, 1694-1714, https://doi.org/10.1109/JSTARS.2018.2812796, 2018.

Romijn, E., Lantican, C. B., Herold, M., Lindquist, E., Ochieng, R., Wijaya, A., Murdiyarso, D., and Verchot, L.: Assessing change in national forest monitoring capacities of 99 tropical countries, For. Ecol. Manage., 352, 109-123, https://doi.org/10.1016/j.foreco.2015.06.003, 2015.

Seidel, D., Annighöfer, P., Thielman, A., Seifert, Q. E., Thauer, J.-H., Glatthorn, J., Ehbrecht, M., Kneib, T., and Ammer, C.: Predicting Tree Species From 3D Laser Scanning Point Clouds Using Deep Learning, Frontiers in Plant Science, Volume 12 - 2021, https://doi.org/10.3389/fpls.2021.635440, 2021.

Shao, J., Park, S., Zhao, C., Habib, A., and Fei, S.: Super-Resolution of Airborne Laser Scanning Point Clouds for Forest Inventory, arXiv preprint arXiv:2605.02201, 2026a.

Shao, J., Choi, D. H., Liu, J., Tian, X., Thapa, B., Lee, S., Habib, A., and Fei, S.: A three-stage framework for stand-level automated stem volume estimation in temperate forests using mobile laser scanning, Remote Sens. Environ., 335, 115246, https://doi.org/10.1016/j.rse.2026.115246, 2026b.

Tebaldini, S., d'Alessandro, M. M., Ulander, L. M. H., Bennet, P., Gustavsson, A., Coccia, A., Macedo, K., Disney, M., Wilkes, P., Spors, H.-J., Schumacher, N., Hanuš, J., Novotný, J., Brede, B., Bartholomeus, H., Lau, A., van der Zee, J., Herold, M., Schuettemeyer, D., and Scipal, K.: TomoSense: A unique 3D dataset over temperate forest combining multi-frequency mono- and bi-static tomographic SAR with terrestrial, UAV and airborne lidar, and in-situ forest census, Remote Sens. Environ., 290, 113532, https://doi.org/10.1016/j.rse.2023.113532, 2023.

Thapa, N., Narine, L. L., and Wilson, A. E.: Forest Aboveground Biomass Estimation Using Airborne LiDAR: A Systematic Review and Meta-Analysis, J. For., 123, 389-412, https://doi.org/10.1007/s44392-025-00029-w, 2025.

Verbeeck, H., Bauters, M., Jackson, T., Shenkin, A., Disney, M., and Calders, K.: Time for a Plant Structural Economics Spectrum, Frontiers in Forests and Global Change, Volume 2 - 2019, https://doi.org/10.3389/ffgc.2019.00043, 2019.

https://doi.org/10.5194/essd-2026-632
Preprint. Discussion started: 22 September 2026

Weiser, H., Schäfer, J., Winiwarter, L., Krašovec, N., Fassnacht, F. E., and Höfle, B.: Individual tree point clouds and tree measurements from multi-platform laser scanning in German forests, Earth Syst. Sci. Data, 14, 2989-3012, https://doi.org/10.5194/essd-14-2989-2022, 2022.

Yang, J., Zhang, H., Li, J., Yang, H., Gao, T., Yang, T., Wang, J., Zhang, X., Yun, T., Duanmu, Y., Chen, S., and Shi, Y.: SmartQSM: a novel quantitative structure model using sparse-convolution-based point cloud contraction for reconstruction and analysis of individual tree architecture, ISPRS J. Photogramm. Remote Sens., 232, 712-739, https://doi.org/10.1016/j.isprsjprs.2026.01.011, 2026.

Yazdi, H., Shu, Q., Rötzer, T., Petzold, F., and Ludwig, F.: A multilayered urban tree dataset of point clouds, quantitative structure and graph models, Scientific Data, 11, 28, https://doi.org/10.1038/s41597-023-02873-x, 2024.

Yin, S., Zhou, K., Cao, L., and Shen, X.: Estimating the Horizontal and Vertical Distributions of Pigments in Canopies of Ginkgo Plantation Based on UAV-Borne LiDAR, Hyperspectral Data by Coupling PROSAIL Model, Remote Sens., 14, 715, https://doi.org/10.3390/rs14030715, 2022.

Zhao, C., Fei, S., and Habib, A.: Integrated scan simultaneous trajectory enhancement and mapping (IS2-TEAM) for fine resolution forest inventory using backpack LiDAR, Remote Sens. Environ., 334, 115212, https://doi.org/10.1016/j.rse.2025.115212, 2026.